01 Jan 2021

Novel Adaptive Sampling Algorithm for POD-Based Non-Intrusive Reduced Order Model

Jiachen Wang

Xiaosong Du
Missouri University of Science and Technology, xdnwp@mst.edu

Joaquim R.R.A. Martins

Recommended Citation

J. Wang et al., "Novel Adaptive Sampling Algorithm for POD-Based Non-Intrusive Reduced Order Model," *AIAA Aviation and Aeronautics Forum and Exposition, AIAA AVIATION Forum 2021*, article no. AIAA 2021-3051, American Institute of Aeronautics and Astronautics, Inc., AIAA, Jan 2021.
The definitive version is available at https://doi.org/10.2514/6.2021-3051

AIAA AVIATION Forum
August 2-6, 2021, VIRTUAL EVENT
AIAA AVIATION 2021 FORUM

10.2514/6.2021-3051

Novel Adaptive Sampling Algorithm for POD-based Non-intrusive Reduced Order Model

Jiachen Wang*, Xiaosong Du† and Joaquim R. R. A. Martins‡
University of Michigan, Ann Arbor, MI 48109, USA

The proper orthogonal decomposition (POD) based reduced-order model (ROM) has been an effective tool for flow field prediction in the engineering industry. The sample selection in the design space for POD basis construction affects the ROM performance sensitively. Adaptive sampling can significantly reduce the number of samples to achieve the required model accuracy. In this work, we propose a novel adaptive sampling algorithm, called conjunction sampling strategy, which is based on proven strategies. The conjunction sampling strategy is demonstrated on airfoil flow field prediction within the transonic regime. We demonstrate the performance of the proposed strategy by running 10 trials for each strategy for the robustness tests. Results show that the conjunction sampling strategy consistently achieves higher predictive accuracy compared with Latin hypercube sampling (LHS) and existing strategies. Specifically, under the same computational budget (40 training samples in total), the conjunction strategy reduced the L_2 error by 56.7% compared with LHS. In addition, the conjunction strategy reduced the standard deviation of L_2 errors by 62.1% with a 2.6% increase on the mean error compared with the best existing strategy.

I. Introduction

High fidelity computational fluid dynamics (CFD) simulation has been widely incorporated into engineering applications [1, 2]. However, the computational cost of direct CFD simulation still prohibits the implementation for complex problems, such as optimal design and risk analysis. To overcome these issues, one promising approach is to use surrogate models instead of computationally expensive CFD simulations on the premise of effectively approximating the original problem [3]. Several types of surrogate models have been demonstrated effective in aerodynamics analysis and design optimizations, including projection-based ROM [4, 5], physical-based shape-preserving response prediction [6], gradient-enhanced kriging and mixtures of experts [7].

Reduced-order modeling (ROM) is a type of commonly used surrogates and can be classified into projection-based ROM, convolution-based ROM [8], center manifold theory [9], harmonic balance [10], and other types [11]. The projection-based ROM transforms the full-space output onto a low-rank space by exploring a set of reduced bases. Due to the dimensional reduction, the reduced-order vector is more convenient to be predicted using data-fitting or other mathematical approximation approaches compared with direct prediction in high dimensions. As suggested by Bui-Thanh et al. [4], the set of reduced bases can be constructed through various methods including proper orthogonal decomposition(POD) [12], reduced-basis methods [13], Krylov-subspace methods [14], and approximated balanced truncation [15]. Among these ROM algorithms, POD is widely used due to its straightforward implementation; therefore, we also use POD-based ROM in this work.

ROM methods can be roughly categorized into intrusive ROM and non-intrusive ROM (NI-ROM). Intrusive ROM requires access to the governing equations. In contrast, NI-ROM considers the physics-based simulation model as a black box: the model learned according to the sample outputs through data-driven methods. A comparison of intrusive and NI-ROM was given by Yıldız et al. [16]. In their work, the intrusive ROM gave a reduced representation of the discretized shallow water equation, while the NI-ROM only reduced the solutions. Therefore, the temporal evolution of the dynamics was approximated by intrusive ROM without further data fitting, while the NI-ROM learned the dynamics of the system by operator inference. Both methods achieved the same level of accuracy. The intrusive ROM is a powerful method to learn the underlying feature of time-dependent problems [17], optimize the reduced basis [18], and estimate output error of model reduction[19] while the NI-ROM is widely applied in solving design optimization

*Graduate student, Department of Aerospace Engineering, AIAA member
†Postdoctoral Research Fellow, Department of Aerospace Engineering, AIAA member
‡Professor, Department of Aerospace Engineering, AIAA Fellow

problems [20] and inverse problems [21]. We investigate the proposed algorithm on NI-ROM due to its convenience and straightforwardness for implementation.

The performance is sensitive to training sample snapshots for most data-driven ROM methods, especially when the computational budget is limited. Therefore, adaptive sampling methods, which lead ROM to the required accuracy threshold with the fewest possible samples, have attracted interest and attention [22, 23]. As suggested by Mackman et al. [24], adaptive sampling algorithms are generally categorized into statistical methods and multi-criteria methods based on the formulation of the sampling objective, while in many previous cases, sampling objectives are to approximate the uncertainty of prediction using existing samples. The common approaches of adaptive sampling are summarized by Jin et al. [25]. Statistical methods use stochastic process models to estimate the uncertainty in prediction, which are particularly popular with Gaussian progress regression. Zhang et al. [26] compared Gaussian progress regression, interquartile range and universal prediction distribution as uncertainty measures for adaptive sampling. Multi-criteria methods formulate sampling objectives based on deterministic criteria such as cross-validation error and distances between samples. Kaminsky et al. [27] presented both cross-validation error and local linear approximation approach in an adaptive Voronoi sampling framework. There are also adaptive sampling strategies developed and implemented specifically for POD-based ROM by Braconnier et al. [22] and Guenot et al. [23]. Both algorithms find new samples with the maximum potential of predictive performance improvement of POD-based ROM based on cross-validation error, which we will introduce in the next section.

Guenot et al. [23] proposed two sampling objectives under the same framework. One objective measures the model improvement according to the rotation of the POD basis vectors, while the other measures the improvement through the change in POD coefficients. In this work, we develop a novel adaptive sampling strategy based on these previous efforts. First, we complete a series of parametric studies for each sampling strategy and investigate the configurations that achieve the best predictive performance. Then, we combine the two sampling strategies at their best setups and switch the sampling objectives at a fixed step in the sampling process. Our results show promising reductions in predictive error under the same computational budget compared with the previous work. We also proposed a new sampling objective, which attempts to combine the two previous objectives, and demonstrated it in the conjunction sampling. However, this new objective does not improve the predictive performance.

The rest of this paper is organized as follows. Section II introduces the methodology used in this work. In particular, Section II.A details the POD-based ROM setup, including model accuracy and parameter space model. Section II.B details the adaptive sampling procedures followed by showing the existing sample algorithms in Section II.C and the proposed sampling strategy in Section II.D. Section III describes the airfoil test cases and compares the proposed sampling strategy with random sampling and previous strategies. This paper ends with conclusion in Section IV.

II. Methodology

This section describes the basics of POD and the general process for adaptive sampling. Then we detail the typical strategies [23] and the proposed novel algorithm in this work.

A. POD-based reduced order model

The proper orthogonal decomposition (POD) is also known as the principal component analysis and the Karhunen-Loeve decomposition. It is a standard tool to extract a low-rank approximation of high dimensional processes and data. The POD reduced order model approximates the high dimensional snapshot vector s by the linear combination of its projections on a set of orthonormal reduced basis vectors ϕ

$$s = \bar{s} + \Sigma_{i=1}^{p} \alpha_i \phi_i, \tag{1}$$

where $\bar{s}$ is the mean of the training snapshots, a_i is the corresponding POD coefficients and p is the number of POD modes included in the ROM. The advantage of the POD-based reduced modeling results from the reduced space, which reveals the underlying structure of the output space to improve the predictive performance.

The reduced basis vectors are generated using the singular value decomposition (SVD) on training data samples. The key step of constructing a ROM is to predict the unknown coefficients (a) with respect to the input parameters. We set up a radial basis function neural network (RBFNN) model to capture the mapping between input parameters and POD coefficients. We use the RBFNN to predict the POD coefficients during the adaptive sampling iterations in this work. Thus, once POD bases and the RBFNN model are constructed, the data-driven modeling of the full states with respect to the input parameters is achieved.

Here we define and explain the notations and details of the POD-based ROM. The parameter space, also called design space, Ω in this paper, specifies the input parameters of the dimension n. The solution space of the CFD simulation has m degrees of freedom, where $m >> n$. In this paper, we work on the two-dimensional design space defined by the angle of attack (α) and Mach number (M). The sample ν is a point in the design space Ω and specifies one pair of α and M. The CFD solution $s(\nu_i)$ is the converged CFD simulation from ADflow [28] with sample ν_i as the parameter. Our sampling strategy is to select samples in the design space to construct a set of POD basis vectors that minimize the error in approximating unknown states. For a set Q of training samples ν in the design space Ω, the CFD solution $s(\nu_i)$ are stacked column by column to formulate a snapshot matrix S as follows

$$S = [s_1, s_2, ...s_k] = [s(\nu_1), s(\nu_2), ...s(\nu_k)], \tag{2}$$

and we formulate the deviation matrix as

$$D = [s_1 - \bar{s}, s_2 - \bar{s}, ..., s_k - \bar{s}]. \tag{3}$$

Then we leverage truncated SVD method on matrix D to produce unitary matrices U and V, and diagonal matrix Σ

$$D = U\Sigma V^T, U \in \mathbb{R}^{m\times n}, \Sigma \in \mathbb{R}^{n\times n}, V \in \mathbb{R}^{n\times n}, m >> n. \tag{4}$$

The matrix U gives the POD basis vector $[\phi_1, ..., \phi_k]$, which are orthogonal vectors. The diagonal matrix Σ includes the singular values in descending order on its diagonal.

The POD coefficients of training data are given as follows

$$a = [a_1, a_2, ..., a_k] = D^T U = V\Sigma, a_i \in \mathbb{R}^n, \tag{5}$$

which states that the POD coefficients can be obtained through Galerkin projection or matrix multiplication of singular values and the right singular vectors. Therefore, the recovered flow states are given as

$$\tilde{s_i} = \bar{s} + \Sigma_{j=1}^{p} a_j \phi_j, p \leq k, \tag{6}$$

which has discrete a values. This set of POD coefficients a is used to train the parameter model and to check the error due to the lack of basis richness. Here we use $q = k$ so that we don't truncate the less dominant POD modes because Guenot et al. [23] suggests that the adaptive sampling doesn't decrease the truncation error in comparison to randomized sampling. The predicted flow states with parameter μ can also be obtained by

$$\tilde{s}(\mu) = \bar{s} + \Sigma_{j=1}^{p} \hat{a}(\mu)_j \phi_j, \mu \in \Omega, \mu \notin Q, \tag{7}$$

where $\hat{a}$ is the predicted coefficient by the RBFNN model and is used during adaptive sampling iterations.

1. Model accuracy

The error the POD model has three sources: lack of basis richness error, truncation error and modeling error. In this paper, we only consider lack of richness error

$$\left\|\delta(\mu)\right\| = \left\|s(\mu) - \tilde{s}(\mu)\right\|. \tag{8}$$

The lack of basis richness error is introduced because the reduced basis vectors do not represent the entire high-dimensional solution space well. Adding new samples into the training set enriches the bases so that more features in the original states can be captured to reduce the richness error. We use this L_2 metric to represent the errors in the results.

2. Radial basis function neural network

RBFNN is implemented as the parameter space model to predict the POD coefficients with respect to the input parameters. This model has the advantages of simple design, good generalization, and robustness against input noise [29, 30]. The RBFNN is a simple neural network with one hidden layer with radial basis function (RBF) as the activation function as follows

$$y(x) = \Sigma_{i=1}^{q} w_i h(\|x - x_i\|_2, \sigma_i). \tag{9}$$

where x is input parameter, y is the quantity of interest, q is number of hidden units, w_i is the RBF weights, x_i is RBF centers, and $\sigma_i$is width. Here we use a Gaussian RBF kernel $h(\cdot)$ for the model. We use the same number of hidden units as the number of POD coefficients, such that $q = k$.

The training process of the RBFNN is the same for each model training: the leave-one-out procedure only changes the set of training samples. We use the RBFNN layer developed by Vidnerova[31] within `Tensorflow` [32]. We use mean square error as loss function and RMSprop as optimizer. Each training process runs 1500 epochs with a training validation split of 85% and 15%.

B. Adaptive sampling procedures

1. Framework

We use the framework proposed by Guenot et al. [23] which is summarized in Algorithm 1. We first randomly generate a set of initial input samples using Latin Hypercube sampling (LHS), then run CFD simulations to obtain the solution snapshots and stack them into the snapshot matrix S_ν. During the sampling, the existing samples are the samples ν with CFD solution snapshot $s(\nu)$ in the snapshot matrix S_ν. The adaptive sampling process determines which candidate is to be added as ν_{new}. For each sampling iteration, a candidate set of new samples μ is generated over the LHS method's design space. The influence factor of each existing sample $infl_\nu$ are computed according to adaptive sampling strategies, which are described in Section II.C. Then each sample candidate μ^i is matched to its closest neighbor ν_n^i in the existing samples ν through a nearest neighbor search. The potential of improvement of the candidates $pot(\mu^i)$ is evaluated as a function of the distance $d(\mu^i, \nu_n^i)$ between the candidate μ^i, and its nearest existing neighbor ν_n^i, and the influence factor of this neighbor. This step is to balance the explore-exploit behavior of sampling. The candidate with the maximum potential of improvement is selected as the new sample (ν_{new}). Its corresponding CFD snapshot vector s_{new} is added to the snapshot matrix. This framework assumes that the influence factor is a continuous function in the parameter space; therefore, as the sample candidate approaches an existing sample, its influence factor value also approaches the influence factor of that existing sample. This assumption enables a nearest-neighbor search in the potential of improvement evaluation which gives an explore-exploit balance.

According to the previous work [23], the number of new sample candidates is suggested as 100 times the input dimensions. Here we suggest a larger number of candidates, which is 500 times the input dimensions, to reduce the uncertainty within the adaptive sampling iteration.

Initial sampling: ν_{LHS}, $S_\nu = S_{LHS}$;
while *Not converged* **do**
  Candidate sampling: μ;
  Influence factor evaluation: $infl(\nu_i) = infl(\nu_i, S_\nu, ...)$;
  Nearest neighbor search: $\nu_n^i = argmin_\nu d(\mu^i, \nu)$;
  Potential of improvement evaluation:$pot(\mu^i) = d(\mu^i, \nu_n^i) infl(\nu_n^i)$;
  Candidate selection: $\nu_{\text{new}} = argmax_\mu pot(\mu)$;
  CFD simulation: s_{new};
  Add ν_{new}, s_{new} to ν and S_ν
end
Result: ν, S_ν

Algorithm 1: adaptive sampling framework

2. Leave-one-out process

The sampling objectives use the leave-one-out (LOO) process to determine the influence factor of each sample by leaving out the sample. For instance, the LOO snapshot matrix with the j^{th} sample left out is denoted as

$$D^{-j} = [s_1 - \bar{s}, ..., s_{j-1} - \bar{s}, -\bar{s}, s_{j+1} - \bar{s}, ...s_k - \bar{s}], \tag{10}$$

through which we construct the LOO POD basis vector with the j^{th} sample left out as

$$U^{-j}\Sigma^{-j}V^{-j^T} = D^{-j}. \tag{11}$$

The LOO procedure for POD coefficients of training set with the j^{th} sample left out denoted as a^{-j}

$$a^{-j} = \begin{bmatrix} a_1^1 & \dots & a_l^1 \\ a_1^2 & \dots & a_l^2 \\ \dots & \dots & \dots \\ a_1^{j-1} & \dots & a_l^{j-1} \\ a_1^{j+1} & \dots & a_l^{j+1} \\ \dots & \dots & \dots \\ a_1^n & \dots & a_l^k \end{bmatrix}. \tag{12}$$

Therefore, the predicted POD coefficients of sample μ through RBFNN is denoted as

$$\hat{a}^{-j}(\mu) = [\hat{a}^{-j}(\mu)_1, ..., \hat{a}^{-j}(\mu)_l]. \tag{13}$$

C. Adaptive sampling objectives

1. Sampling objective A: influence factor based on POD basis

This sampling objective is based on the rotation of POD basis due to the addition of each sample. The influence factor on the POD basis of the i^{th} sample $infl_{Basis}(\nu_i)$ is defined as

$$infl_{Basis}(\nu_i) = \Sigma_{j=1}^{l} \sigma_j \left(\frac{1}{\left|\phi_j \cdot \phi_j^{-i}\right|} - 1\right), \tag{14}$$

where the dot product gives the cosine value to the angle between the original POD basis and the LOO POD basis. The parameter l gives the number of POD modes which are considered improved in the ROM. Note that l is not related to p and therefore not relevant to the truncation of the POD modes, however, typically $l \leq q$. If removing one sample causes a large rotation angle of the dominant POD basis, the influence factor of this sample is large. The relative influence factor on POD basis of the i^{th} sample is given as

$$infl_{Basis}^{Rel}(\nu_i) = \frac{infl_{Basis}(\nu_i)}{\Sigma_{k=1}^{n} infl_{Basis}(\nu_k)}, \tag{15}$$

which scales $infl_{Basis}^{Rel}(\nu_i)$ based on the singular values to weight the influence of each POD basis.

To further reduce the computational cost of the truncated SVD operation, we used the following theorem [23]

$$\left|\phi_j \cdot \phi_j^{-i}\right| = \left|U_n[i,i]\right|, \text{where } U_n \Sigma_n V_n^T = \Sigma(I - V[j,:]^T V[j,:]). \tag{16}$$

2. Sampling objective B: influence factor based on POD coefficients

This sampling objective is based on the change of POD coefficients due to the addition of each sample. This sampling objective has two sub-strategies: improve all POD modes or improve the mode with the worst parameter space model. The sub-strategy of each sampling iteration is determined by the correlation between the current and the predicted POD coefficients of the existing samples. The correlation of the POD coefficient of the i^{th} mode is evaluated by

$$corr(\hat{a_i}) = \frac{n\Sigma_{j=1}^{n}(a_i)_j \hat{a}(\nu_j)_i - \Sigma_{j=1}^{n}(a_i)_j \Sigma_{j=1}^{n} \hat{a}(\nu_j)_i}{\sqrt{n\Sigma_{j=1}^{n}[(a_i)_j]^2 - [\Sigma_{j=1}^{n}(a_i)_j]^2}\sqrt{n\Sigma_{j=1}^{n}\hat{a}(\nu_j)_i{}^2 - (\Sigma_{j=1}^{n}\hat{a}(\nu_j)_i)^2}}. \tag{17}$$

And the weighted quality of the POD coefficient of the i^{th} mode as

$$WQ(\hat{a_i}) = \left(\frac{\sigma_i}{\Sigma_{j=1}^{K}\sigma_j}\right) corr(\hat{a_i}) \tag{18}$$

Then if the correlation of POD coefficient with the minimum weighted quality is less than 0.7, the POD coefficient with the lowest weighted quality is selected for influence factor evaluation following the one-mode-at-a-time sub-strategy as

$$infl(a_i) = \left| (a_i)_j - \hat{a}^{-j}(v_j)_i \right|. \tag{19}$$

Otherwise, the POD coefficients of all modes are improved following the altogether sub-strategy as

$$infl^{Rel}_{Coeff} = \frac{infl_{Coeff}(v_j)}{\Sigma_{k=1}^{n} infl_{Coeff}(v_k)}, \tag{20}$$

where

$$infl_{Coeff}(v_j) = \Sigma_{i=1}^{l} \sigma_i infl_{a_i}(v_j). \tag{21}$$

However, the POD coefficient selection based on correlation is not effective for regression models like Gaussian process regression, which has a constant correlation of 1. In this paper, we used the RBFNN as the regression model. Another significant drawback of this sampling objective is the computational cost. The computational cost of this objective function is significantly higher than objective A because the LOO procedure trains the model as many times as the number of samples for each sampling iteration.

3. Sampling objective C: influence factor based on error vector in reduced space

To consider both the rotation of the POD basis and the change in POD coefficients due to the addition of each sample, we propose a formulation based on the error vector in the POD reduced space. The LOO error vector for each POD mode is defined as

$$\vec{e_i}(v_j) = (a_i)_j \phi_i - \hat{a}^{-j}(v_j)_i \phi_i^{-j}. \tag{22}$$

To evaluate the norm of error vector without using the high dimensional vectors ϕ_i and ϕ_i^{-j}, we decomposed ϕ_i^{-j} into a parallel component and a vertical component of ϕ_i (Fig. 1). The norm of these two components are straightforward to calculate if the angle θ between ϕ_i and ϕ_i^{-j}

Therefore, we use the L_2 norm of the error vector as the influence factor. We use the similar definition of weighted quality and the same sub-strategies as objective B. The threshold value of the weighted quality to switch between the sub-strategies is set as 0.7, same as objective B. The one-mode-at-a-time sub-strategy is defined as

$$infl_i(v_j) = d_{L_2}\left(\left(0, \left\| \vec{e_\perp^i} \right\| \right), \left(\left\| \vec{e_\parallel^i} \right\|, 0 \right) \right), \tag{23}$$

where d_{L_2} measures the L_2 distance. And the altogether sub-strategy is defined as

$$infl(v_j) = \Sigma_{i=1}^{l} infl_i(v_j). \tag{24}$$

The altogether sub-strategy doesn't use the singular values to weigh the error in each POD mode because the singular value is already included in the POD coefficients. The drawback of this objective is the same as objective B since it has the same sub-strategies and includes the change in POD coefficients due to the addition of a sample.

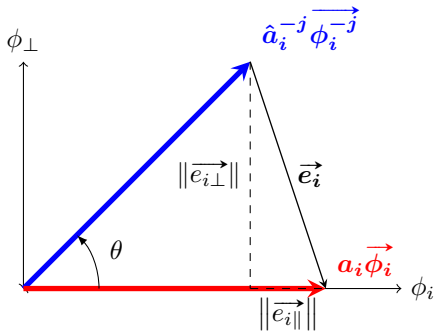

Fig. 1 LOO error vector in reduced space spanned by the POD basis

D. Conjunction sampling strategies

Because the aforementioned two adaptive sampling strategies are independent and separate processes, we propose a conjunction adaptive sampling algorithm so that both the POD basis and the coefficients are considered in the sampling process. Thus, we can improve the ROM predictive performance and lower the computational cost of adaptive sampling objectives. This new sampling strategy consists of two stages, each of which uses a different sampling objective and includes multiple sampling iterations. The switch between the two stages is currently at a step determined a priori. Therefore, the conjunction adaptive strategy improves both the POD basis and the POD coefficients at different stages to generate one set of samples.

The order of the sampling objectives is critical for the performance of the POD model. To improve the precision of the POD-based ROM, objective A shall be run at the first stage since the basis rotation is more significant at the earlier stage of sampling.

III. Results

In this section, we demonstrate the proposed algorithm on a typical airfoil case set up by the AIAA Aerodynamic Design Optimization Discussion Group (ADODG). A series of comparisons against existing adaptive sampling objectives reveal the promising performance of the conjunction strategy.

A. Problem formulation

ADODG case 2 considers transonic viscous flow over the RAE 2822 airfoil. Specifically, the case has the following flight conditions: $M = 0.734$, $C_l^* = 0.824$, and a Reynolds number of 6.5×10^6. We formulate our test cases by setting M uniformly distributed as $\mathcal{U}(0.55, 0.75)$ and α as $\mathcal{U}(-1, 3)$ since M and α have major effects on the flow fields. And we will not consider C_l^* since we are not doing optimization in the current work.

B. Grid convergence study

We complete a grid convergence study (Fig. 2) based on the Richardson extrapolation (RE) algorithm. Provided with C_d values from multi-fidelity simulation models, the RE algorithm approximates the C_d for an infinite number of mesh cells which we use to check the effectiveness of simulation models. Results show the C_d difference between $L1$ model and RE approximation is around 0.5 drag count (10^{-4}). Considering the computational cost, we select the $L1$ model as the high-fidelity model in this work.

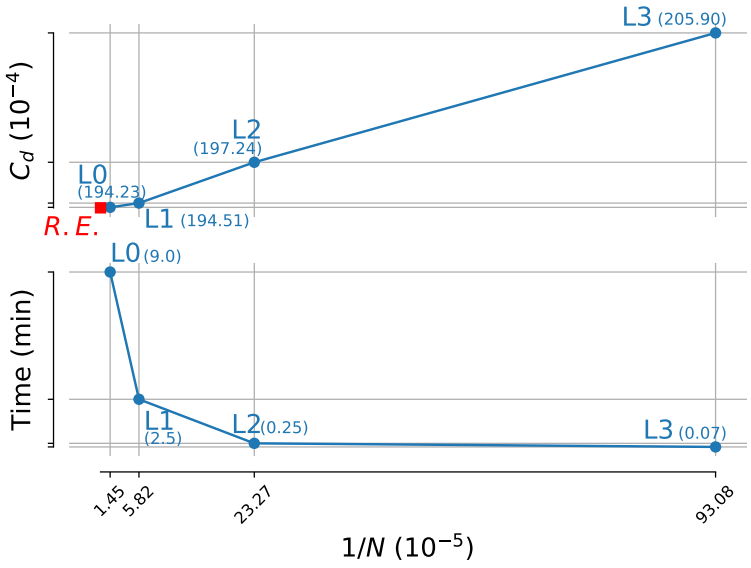

Fig. 2 Grid convergence study shows that $L1$ model has a C_d difference of around 0.5 drag count compared with the RE approximation, and takes 2.5 minutes for one simulation using 96 cores.

C. Results comparison

In this work, we first investigate the adaptive sample selection for each adaptive sampling strategy. Then we use the best setups for each strategy to construct the conjunction algorithm and complete a series of parametric studies. For each sampling strategy, we run 10 trials with the same set of 16 initial LHS samples.

The performance of the adaptive sampling strategies is evaluated according to the mean value and standard deviation of the L_2 error (Eq. 8) of reconstructing the testing flow states. The testing flow states are 121 uniform-distributed samples in the design space with $\Delta M = 0.02, \Delta\alpha = 0.4^o$. The flow states are reconstructed via matrix multiplication on all 40 POD basis vectors. Therefore, we are only comparing the error due to the lack of basis richness as defined in Eq. 8. The L_2 error of each trial is the average L_2 errors of the reconstructed testing flow states.

The sampling strategies are denoted as capitalized letters followed by the number in parenthesis. The capitalized letter indicates the sampling objective, whereas the number in parenthesis indicates the number of samples generated from the corresponding sampling objective. The subscript $_1$ indicates that we consider the first 8 POD modes in the corresponding sampling objective, whereas subscript $_2$ indicates all available POD modes in the corresponding sampling objective. For instance, $A_2(18)B_1(6)$ indicates that the conjunction sampling scheme generates 18 samples in the first stage with objective A, then generates 6 samples in the second stage with objective B. Objective A considers all POD bases available, whereas objective B considers the first 8 POD modes.

1. Investigation on existing sampling objectives

The previous work by Guenot et al. [23] selected all adaptive samples according to a single objective with a fixed number of POD modes. We compare this approach with the strategy of using all available POD modes within every iteration (Fig. 3). Cases $A_1(24)$ and $B_1(24)$ have the influence factor evaluated using the first 8 POD modes. Cases $A_2(24)$ and $B_2(24)$ have the influence factor evaluated using all available POD modes.

Case $A_2(24)$ yields the lowest mean L_2 error among the 4 cases for single objective sampling. Therefore we use objective A with all POD modes for the first stage of conjunction sampling. Case $B_2(24)$ yields the worst performance in both mean and standard deviation of L_2 error, which is consistent with the result of the previous work [23]: objective B is sensitive to the number of POD modes. As shown in Fig. 6e, the adaptive samples barely cluster toward the region with high error for flow states reconstruction in the design space.

2. Conjunction adaptive sampling

The performances of the conjunction adaptive sampling strategies are summarized in Fig. 4. We test the conjunction sampling combinations of objective A, where all the POD modes are improved, followed by objective B or objective C, where the first 8 modes are improved. The conjunction sampling strategy with objective B performs better overall than objective C in both mean and standard deviation L_2.

In Fig. 5 we test a conjunction sampling strategy with a range of the number of the samples generated by each sampling objective. We observe that the performance of the sampling strategy is not monotonic according to the number of samples in the first step. The strategy $A_2(18)B_1(6)$ has the lowest standard deviation of L_2 error among all the test cases and has hte second-lowest mean L_2 error of 7.01×10^{-4}.

Overall, the best results are from all 24 samplings using objective A with all POD modes improved ($A_2(24)$) and 18 samples using objective 1 improving all modes followed by 6 samples using objective 2 improving the first 8 modes

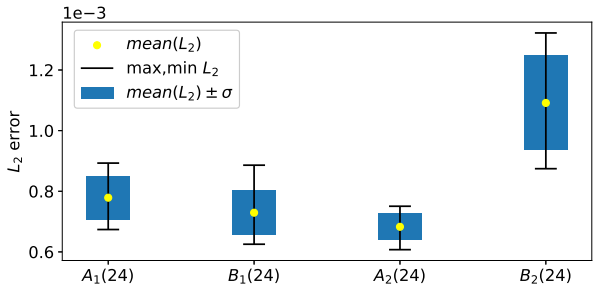

Fig. 3 Performance of single objective sampling based on L_2 error

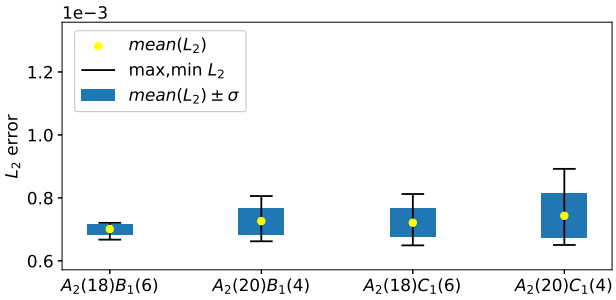

Fig. 4 Performance of conjunction adaptive sampling based on L_2 error

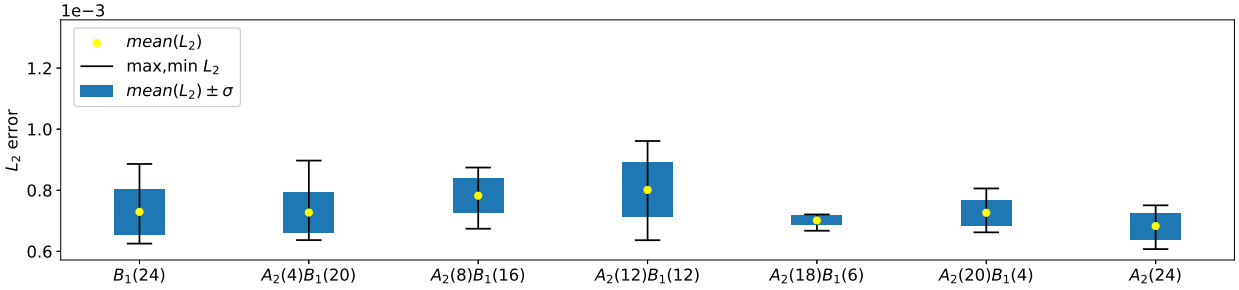

Fig. 5 Parametric study of conjunction adaptive sampling strategies

($A_2(18)B_1(6)$). The conjunction sampling algorithm ($A_2(18)B_1(6)$) has 2.6% higher mean but 62.1% lower standard deviation of L_2 error than the objective A with all POD modes improved ($A_2(24)$). Since most real-world applications run the sampling only once, the conjunction sampling algorithm is a better approach due to the very low standard deviation in error.

To obtain richer insights into the results, we present the sample pattern with the minimal L_2 error among the 10 trials in Fig. 6 for each sampling strategy. We can see that the adaptive sampling strategies tend to add more points at the high-M and high-α region, which is highly nonlinear. Thus, the predictive performance of ROM models can be improved as expected.

Figures 7 to 11 show the flow states provided by CFD simulation, the LHS samples, and the adaptive samples by $A_2(18)B_1(6)$. This set of adaptive samples is from the trial with close-to-average performance among the 10 trials using the same strategy. The flow fields from CFD simulations are shown in Fig. 7. The flow states reconstruction with LHS samples and with $A_2(18)B_1(6)$ samples are shown in Fig. 8 and Fig. 9 respectively. Both sets of samples give good approximations of the flow states. We further compare the predictive performance by showing the corresponding errors in Fig. 10 and Fig. 11. The error from the $A_2(18)B_1(6)$ is significantly lower than the other case at the location of the shock wave, indicating the flow feature is better captured by this strategy.

IV. Conclusion

Existing adaptive sampling [23], a new influence factor formulation, and the proposed conjunction adaptive strategy are demonstrated in this work. We first investigate the performance of each strategy to guide the POD basis construction. Then we compare the conjunction strategy with single strategies at the best performance.

All the sampling strategies are demonstrated on airfoil cases in transonic flow. Results show that, with the same initial sample set and the same number of adaptive samples, the POD bases from the conjunction sampling strategy significantly improves the predictive accuracy compared with the Latin hypercube sampling. In terms of robustness tests using 10 different trials, the conjunction algorithm shows higher consistency achieving accurate flow field reconstruction than that of the best single sampling objectives.

We conclude that conjunction adaptive sampling strategy has promising potential in more generalized engineering applications. However, the number of samples at each strategy stage remains quantitatively undetermined. We are

planning to set up a more intelligent way of switching between strategies and demonstrate this conjunction algorithm on more test cases.

Acknowledgments

The authors acknowledge the Texas Advanced Computing Center (TACC) at The University of Texas at Austin for providing high-performance computing resources that have contributed to the research results reported within this paper. URL: http://www.tacc.utexas.edu

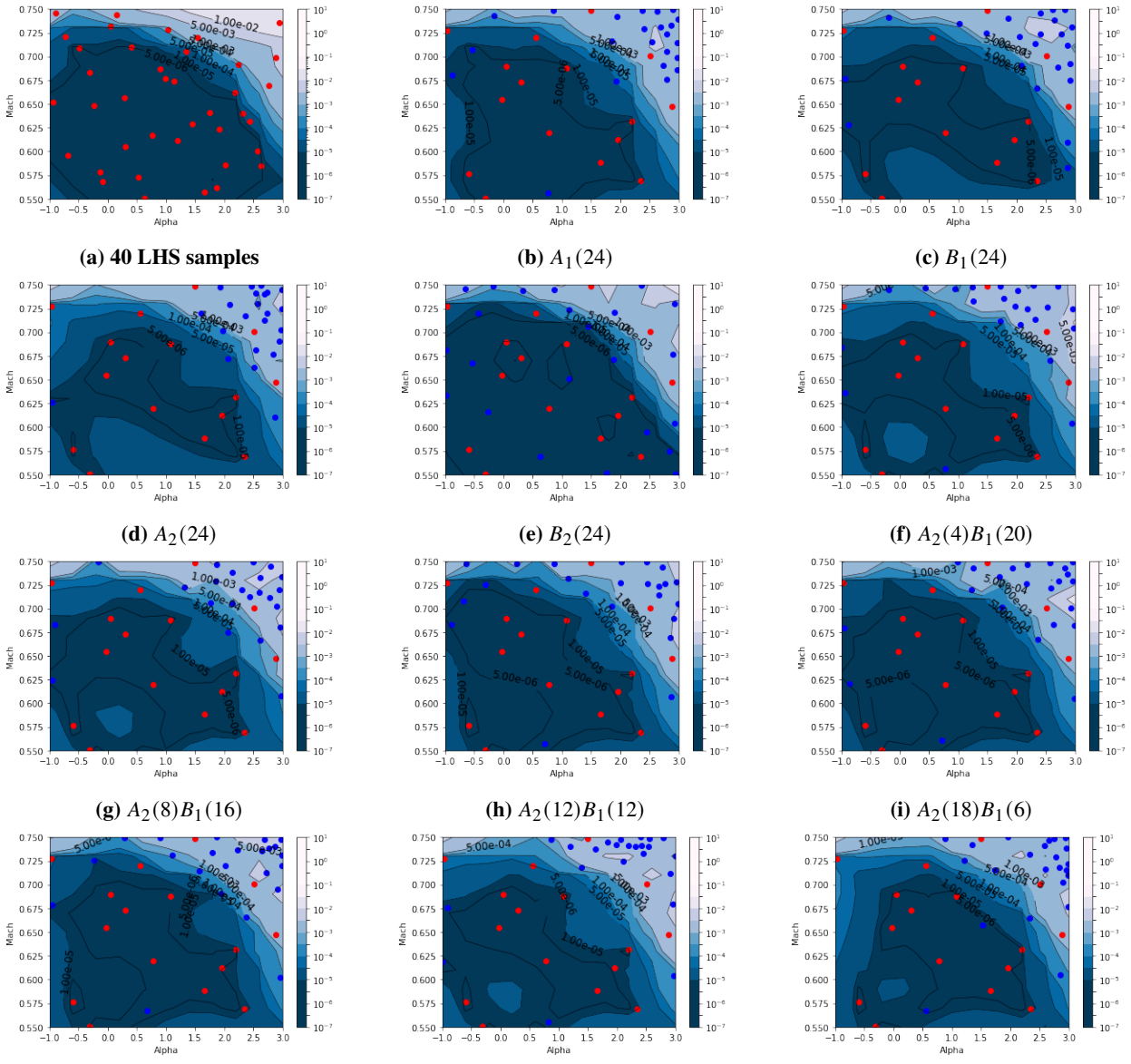

(a) 40 LHS samples **(b)** $A_1(24)$ **(c)** $B_1(24)$

(d) $A_2(24)$ **(e)** $B_2(24)$ **(f)** $A_2(4)B_1(20)$

(g) $A_2(8)B_1(16)$ **(h)** $A_2(12)B_1(12)$ **(i)** $A_2(18)B_1(6)$

(j) $A_2(20)B_1(4)$ **(k)** $A_2(18)C_1(6)$ **(l)** $A_2(20)C_1(4)$

Fig. 6 Sampling patterns of LHS and 11 sampling strategies

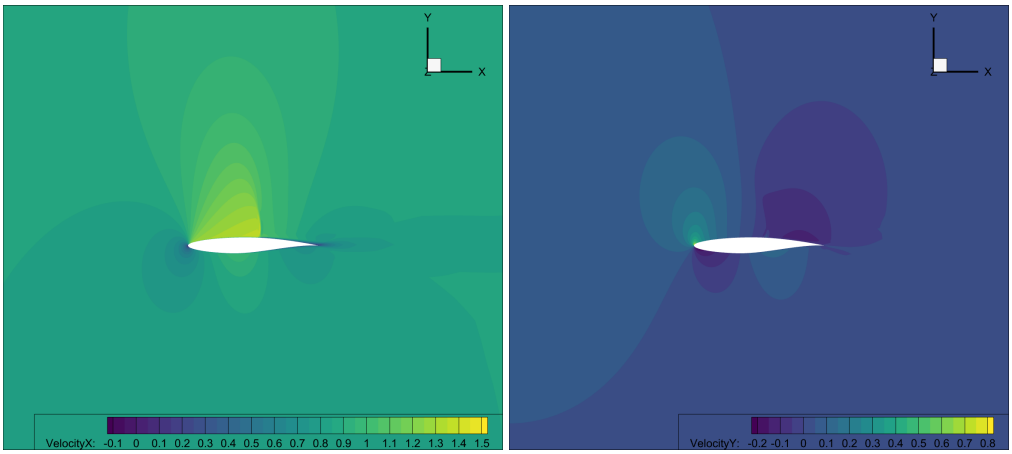

(a) **(b)**

Fig. 7 Flow fields by CFD simulation at $M = 0.73, \alpha = 2.6^o$.

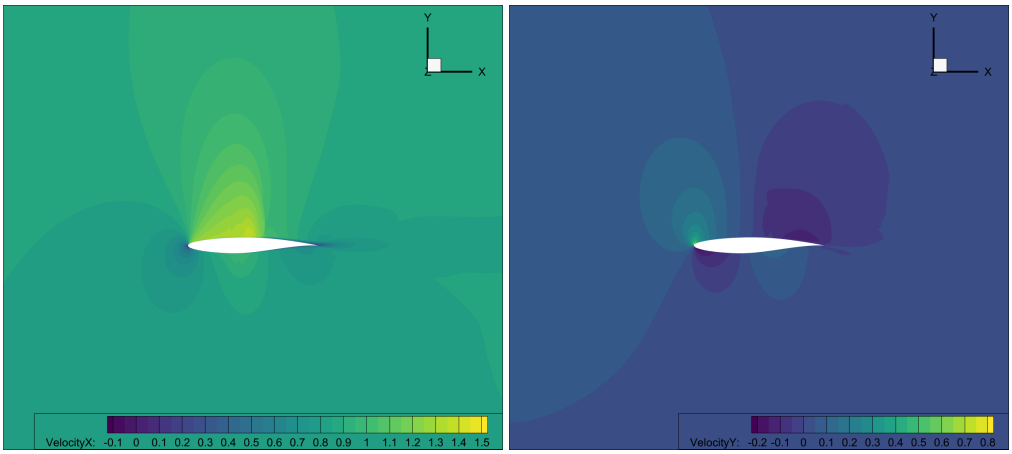

(a) **(b)**

Fig. 8 Flow states reconstruction with 40 LHS samples.

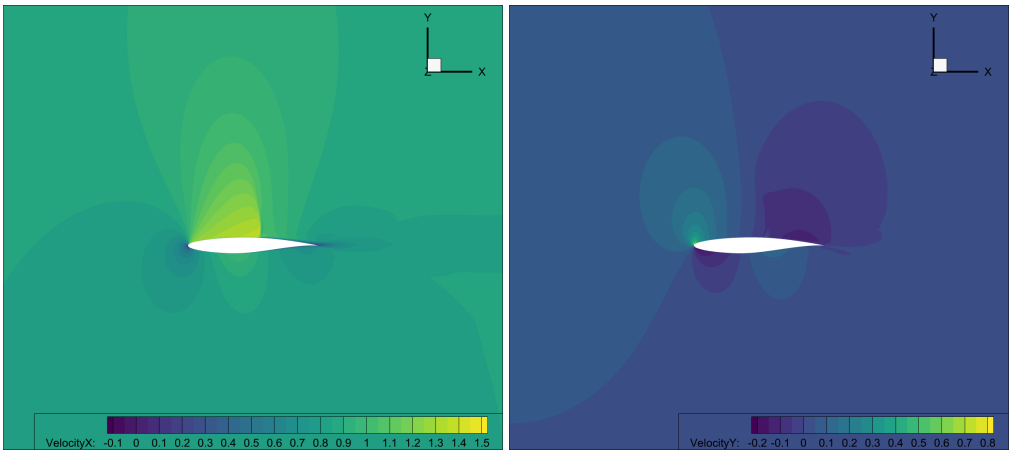

(a) **(b)**

Fig. 9 Flow states reconstruction with $A_2(18)B_1(6)$ samples

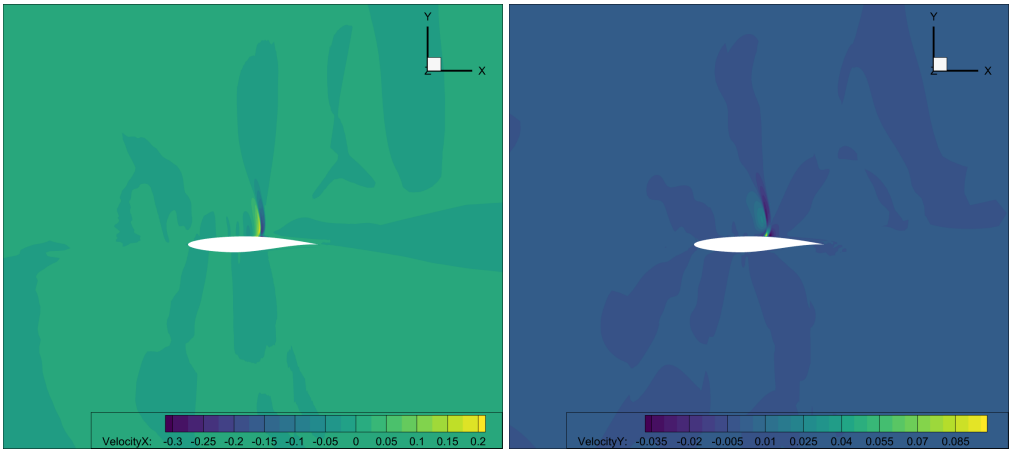

(a) **(b)**

Fig. 10 Error in flow states reconstruction with 40 LHS samples.

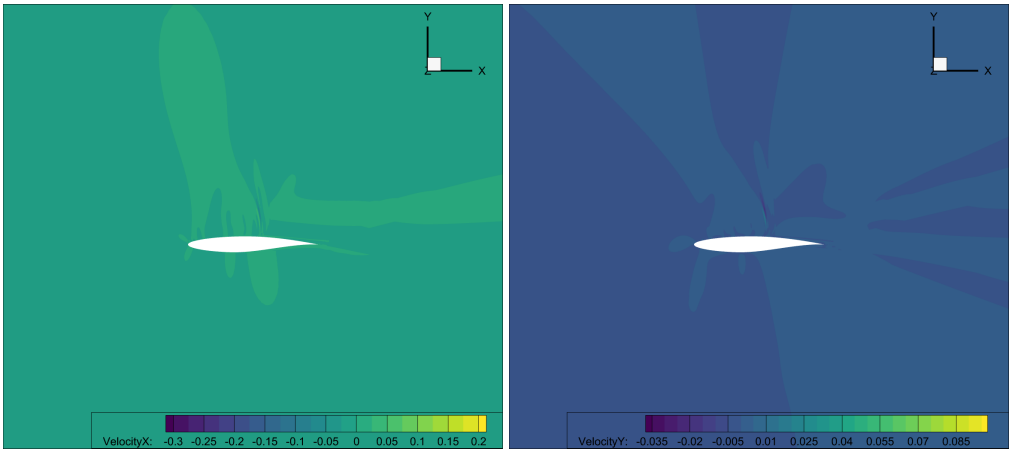

(a) **(b)**

Fig. 11 Error in flow states reconstruction with $A_2(18)B_1(6)$ samples.

References

[1] Lyu, Z., Kenway, G. K. W., and Martins, J. R. R. A., "Aerodynamic Shape Optimization Investigations of the Common Research Model Wing Benchmark," *AIAA Journal*, Vol. 53, No. 4, 2015, pp. 968–985. https://doi.org/10.2514/1.J053318.

[2] Martins, J. R. R. A., "Perspectives on Aerodynamic Design Optimization," *AIAA SciTech Forum*, AIAA, Orlando, FL, 2020. https://doi.org/10.2514/6.2020-0043.

[3] Martins, J. R. R. A., and Ning, A., *Engineering Design Optimization*, Cambridge University Press, 2021. https://doi.org/10.1017/9781108980647, URL https://www.researchgate.net/publication/352413464_Engineering_Design_Optimization.

[4] Bui-Thanh, T., Willcox, K., and Ghattas, O., "Parametric reduced-order models for probabilistic analysis of unsteady aerodynamic applications," *AIAA journal*, Vol. 46, No. 10, 2008, pp. 2520–2529.

[5] He, P., Halder, R., Fidkowski, K., Maki, K., and Martins, J. R. R. A., "An efficient nonlinear reduced-order modeling approach for rapid aerodynamic analysis with OpenFOAM," *AIAA Scitech 2021 Forum*, 2021. https://doi.org/10.2514/6.2021-1476.

[6] Leifsson, L., and Koziel, S., "Multi-fidelity design optimization of transonic airfoils using physics-based surrogate modeling and shape-preserving response prediction," *Journal of Computational Science*, Vol. 1, No. 2, 2010, pp. 98–106. https://doi.org/https://doi.org/10.1016/j.jocs.2010.03.007, URL https://www.sciencedirect.com/science/article/pii/S1877750310000098.

[7] Liem, R. P., Mader, C. A., and Martins, J. R., "Surrogate models and mixtures of experts in aerodynamic performance prediction for aircraft mission analysis," *Aerospace Science and Technology*, Vol. 43, 2015, pp. 126–151. https://doi.org/https://doi.org/10.1016/j.ast.2015.02.019, URL https://www.sciencedirect.com/science/article/pii/S1270963815000760.

[8] Balajewicz, M., Nitzsche, F., and Feszty, D., "Application of Multi-Input Volterra Theory to Nonlinear Multi-Degree-of-Freedom Aerodynamic Systems," *AIAA Journal*, Vol. 48, No. 1, 2010, pp. 56–62. https://doi.org/10.2514/1.38964, URL https://doi.org/10.2514/1.38964.

[9] Woodgate, M. A., and Badcock, K. J., "Fast Prediction of Transonic Aeroelastic Stability and Limit Cycles," *AIAA Journal*, Vol. 45, No. 6, 2007, pp. 1370–1381. https://doi.org/10.2514/1.25604, URL https://doi.org/10.2514/1.25604.

[10] Lucia, D. J., Beran, P. S., and Silva, W. A., "Reduced-order modeling: new approaches for computational physics," *Progress in Aerospace Sciences*, Vol. 40, No. 1, 2004, pp. 51–117. https://doi.org/https://doi.org/10.1016/j.paerosci.2003.12.001, URL https://www.sciencedirect.com/science/article/pii/S0376042103001131.

[11] Balajewicz, M., and Dowell, E., "Reduced-order modeling of flutter and limit-cycle oscillations using the sparse volterra series," *Journal of Aircraft*, Vol. 49, No. 6, 2012, pp. 1803–1812. https://doi.org/10.2514/1.C031637.

[12] Deane, A. E., Kevrekidis, I. G., Karniadakis, G. E., and Orszag, S. A., "Low-dimensional models for complex geometry flows: Application to grooved channels and circular cylinders," *Physics of Fluids A: Fluid Dynamics*, Vol. 3, No. 10, 1991, pp. 2337–2354. https://doi.org/10.1063/1.857881, URL https://doi.org/10.1063/1.857881.

[13] FOX, R. L., and MlURA, H., "An approximate analysis technique for design calculations," *AIAA Journal*, Vol. 9, No. 1, 1971, pp. 177–179. https://doi.org/10.2514/3.6141, URL https://doi.org/10.2514/3.6141.

[14] Feldmann, P., and Freund, R., "Efficient linear circuit analysis by Pade approximation via the Lanczos process," *IEEE Transactions on Computer-Aided Design of Integrated Circuits and Systems*, Vol. 14, No. 5, 1995, pp. 639–649. https://doi.org/10.1109/43.384428.

[15] Gugercin, S., and Antoulas, A. C., "A Survey of Model Reduction by Balanced Truncation and Some New Results," *International Journal of Control*, Vol. 77, No. 8, 2004, pp. 748–766. https://doi.org/10.1080/00207170410001713448, URL https://doi.org/10.1080/00207170410001713448.

[16] Yıldız, S., Uzunca, M., and Karasözen, B., "Intrusive and non-intrusive reduced order modeling of the rotating thermal shallow water equation," *arXiv:2104.00213 [cs, math]*, 2021. URL http://arxiv.org/abs/2104.00213, arXiv: 2104.00213.

[17] Qian, E., Kramer, B., Peherstorfer, B., and Willcox, K., "Lift & Learn: Physics-informed machine learning for large-scale nonlinear dynamical systems," *Physica D: Nonlinear Phenomena*, Vol. 406, 2020, p. 132401. https://doi.org/10.1016/j.physd.2020.132401, URL http://dx.doi.org/10.1016/j.physd.2020.132401.

[18] Collins, G., Fidkowski, K., and Cesnik, C. E., "Petrov-Galerkin projection-based model reduction with an optimized test space," *AIAA Scitech 2020 Forum*, 2020, p. 1562.

[19] Collins, G., Fidkowski, K., and Cesnik, C. E., "Output Error Estimation for Projection-Based Reduced Models," *AIAA Aviation 2019 Forum*, 2019, p. 3528.

[20] Iuliano, E., and Quagliarella, D., "Aerodynamic shape optimization via non-intrusive POD-based surrogate modelling," *2013 IEEE Congress on Evolutionary Computation*, IEEE, 2013, pp. 1467–1474.

[21] Bui-Thanh, T., Damodaran, M., and Willcox, K., "Aerodynamic data reconstruction and inverse design using proper orthogonal decomposition," *AIAA journal*, Vol. 42, No. 8, 2004, pp. 1505–1516.

[22] Braconnier, T., Ferrier, M., Jouhaud, J.-C., Montagnac, M., and Sagaut, P., "Towards an adaptive POD/SVD surrogate model for aeronautic design," *Computers & Fluids*, Vol. 40, No. 1, 2011, pp. 195–209.

[23] Guenot, M., Minisci, E., Quagliarella, D., Guénot, M., Lepot, I., Sainvitu, C., Goblet, J., and Coelho, R. F., "Adaptive sampling strategies for non-intrusive POD-based surrogates," *Engineering computations*, 2013.

[24] Mackman, T. J., Allen, C. B., Ghoreyshi, M., and Badcock, K. J., "Comparison of Adaptive Sampling Methods for Generation of Surrogate Aerodynamic Models," *AIAA Journal*, Vol. 51, No. 4, 2013, pp. 797–808. https://doi.org/10.2514/1.J051607, URL https://doi.org/10.2514/1.J051607.

[25] Jin, R., Chen, W., and Sudjianto, A., "On sequential sampling for global metamodeling in engineering design," *International design engineering technical conferences and computers and information in engineering conference*, Vol. 36223, 2002, pp. 539–548.

[26] Zhang, Y., Kim, N. H., and Haftka, R. T., "General-surrogate adaptive sampling using interquartile range for design space exploration," *Journal of Mechanical Design*, Vol. 142, No. 5, 2020.

[27] Kaminsky, A. L., Wang, Y., Pant, K., Hashii, W. N., and Atachbarian, A., "Adaptive sampling techniques for surrogate modeling to create high-dimension aerodynamic loading response surfaces," *2018 Applied Aerodynamics Conference*, 2018, p. 4199.

[28] Mader, C. A., Kenway, G. K. W., Yildirim, A., and Martins, J. R. R. A., "ADflow: An Open-Source Computational Fluid Dynamics Solver for Aerodynamic and Multidisciplinary Optimization," *Journal of Aerospace Information Systems*, Vol. 17, No. 9, 2020.

[29] Chenou, J., Hsieh, G., and Fields, T., "Radial Basis Function Network: Its Robustness and Ability to Mitigate Adversarial Examples," *2019 International Conference on Computational Science and Computational Intelligence (CSCI)*, IEEE, 2019, pp. 102–106.

[30] Liu, J., *Radial Basis Function (RBF) neural network control for mechanical systems: design, analysis and Matlab simulation*, Springer Science & Business Media, 2013.

[31] Petra, V., "RBF-Keras: an RBF Layer for Keras Library," https://github.com/PetraVidnerova/rbf_keras, 2019.

[32] Abadi, M., Agarwal, A., Barham, P., Brevdo, E., Chen, Z., Citro, C., Corrado, G. S., Davis, A., Dean, J., Devin, M., Ghemawat, S., Goodfellow, I., Harp, A., Irving, G., Isard, M., Jia, Y., Jozefowicz, R., Kaiser, L., Kudlur, M., Levenberg, J., Mané, D., Monga, R., Moore, S., Murray, D., Olah, C., Schuster, M., Shlens, J., Steiner, B., Sutskever, I., Talwar, K., Tucker, P., Vanhoucke, V., Vasudevan, V., Viégas, F., Vinyals, O., Warden, P., Wattenberg, M., Wicke, M., Yu, Y., and Zheng, X., "TensorFlow: Large-Scale Machine Learning on Heterogeneous Systems," , 2015. URL https://www.tensorflow.org/, software available from tensorflow.org.